Spin and orbital ordering in $La_{2-2x}Sr_{1+2x}Mn_2O_7$ compounds

Qinfang Zhang, Weiyi Zhang, and Zhengsheng Jiang
National Laboratory of Solid State Microstructures and Department of Physics, Nanjing University, Nanjing 210093, China
(Received 31 May 2005; revised manuscript received 26 August 2005; published 18 October 2005)

In this Brief Report, the electronic and magnetic structures of the bilayer Ruddlesden-Popper compounds, $La_{2-2x}Sr_{1+2x}Mn_2O_7$ ($0.0 \leqslant x \leqslant 1.0$), have been investigated using the unrestricted Hartree-Fock approximation and the real-space recursion method. Various ground states are found as a function of Sr doping which reveal an interesting interplay between spin and orbital degrees of freedom. The undoped $La_2Sr_1Mn_2O_7$ takes the A-type antiferromagnetic ground state with $d_{3x^2-r^2}/d_{3y^2-r^2}$ orbital ordering. As doping increases, the ground state of system takes consecutively the ferromagnetic state with $d_{3x^2-r^2}/d_{3y^2-r^2}$ orbital ordering ($0.01 \leqslant x \leqslant 0.23$), the ferromagnetic state with $d_{x^2-y^2}$ orbital ordering ($0.23 < x \leqslant 0.34$), the A-type antiferromagnetic state with $d_{x^2-y^2}$ orbital ordering ($0.34 < x \leqslant 0.86$), the C-type antiferromagnetic state with $d_{x^2-y^2}$ orbital ordering ($0.86 < x \leqslant 0.92$), and finally the G-type antiferromagnetic state with $d_{3z^2-r^2}$ orbital ordering ($0.92 < x \leqslant 1$).

DOI: 10.1103/PhysRevB.72.142401 PACS number(s): 75.25.+z, 75.47.Gk

The discovery of collosal magnetoresistance (CMR) in doped $LaMnO_3$ compound has revived our interest in properties of perovskite oxides.[1–3] Recent studies show that CMR effect[4–6] not only occurs in the cubic structured $La_{1-x}Sr_xMnO_3$ compounds, but also widely appears in other types of manganites. In particular, the $n=2$ member of the Ruddlesden-Popper series of manganites, $La_{2-2x}Sr_{1+2x}Mn_2O_7$,[7] demonstrates excellent low field CMR effect due to its quasi-two-dimensional nature. In $La_{2-2x}Sr_{1+2x}Mn_2O_7$ perovskite, $(La,Sr)MnO_3$ bilayers are stacked between (La, Sr)O blocking layers. The system forms natural quasi-two-dimensional tunneling structures as opposed to the heterostructures obtained by thin film deposition.[8,9] The crystal structure and magnetic phase diagram have been investigated using x-ray diffraction and neutron diffraction by many research groups for various doping range.[7,10–16]. Among others, Kimura *et al.*[10] found that the bilayered $La_{2-2x}Sr_{1+2x}Mn_2O_7$ system is a ferromagnetic metal at narrow doping range $0.32 \leqslant x \leqslant 0.40$; Ling *et al.*[11] determined the magnetic phase diagram at large doping range and a similar trend to the cubic structured perovskite is observed. The doped bilayer perovskite takes the A-type antiferromagnetic state for doping concentration $0.5 \leqslant x \leqslant 0.66$, the C-type antiferromagnetic state for $0.75 \leqslant x \leqslant 0.9$, and the G-type antiferromagnetic state for $0.9 \leqslant x \leqslant 1$. Some theoretical studies have also been carried out on the bilayered perovskites, but they are mainly concentrated on the range around $x \approx 0.5$.[12,13] Thus, there is still a much unexplored region across the whole doping range. Also, the correlation between spin, charge, and orbital orderings remains to be investigated.

To achieve a better physical understanding of the magnetic and orbital properties of $La_{2-2x}Sr_{1+2x}Mn_2O_7$ compounds, we have studied various possible metastable states of $La_{2-2x}Sr_{1+2x}Mn_2O_7$ as a function of Sr doping. Six of them turn out to be metastable and are schematically drawn in Fig. 1. Most importantly, the electronic correlations and Jahn-Teller interaction are treated on equal footing in our study. The three different types of nearest neighbor in-plane orbital orderings, i.e., $d_{3x^2-r^2}/d_{3y^2-r^2}$, $d_{3z^2-r^2}$, and $d_{x^2-y^2}$, are taken into account in all magnetically ordered states. The detailed analysis of these metastable states suggested that as a function of doping, the ground state of $La_{2-2x}Sr_{1+2x}Mn_2O_7$ takes consecutively the A-type antiferromagnetic state with $d_{3x^2-r^2}/d_{3y^2-r^2}$ orbital ordering ($x=0$), the ferromagnetic (FM) state with $d_{3x^2-r^2}/d_{3y^2-r^2}$ orbital ordering ($0.01 \leqslant x \leqslant 0.23$), the ferromagnetic state with $d_{x^2-y^2}$ orbital ordering ($0.23 < x \leqslant 0.34$), the A-type antiferromagnetic state with $d_{x^2-y^2}$ orbital ordering ($0.34 < x \leqslant 0.86$), the C-type antiferromagnetic state with $d_{x^2-y^2}$ orbital ordering ($0.86 < x \leqslant 0.92$),

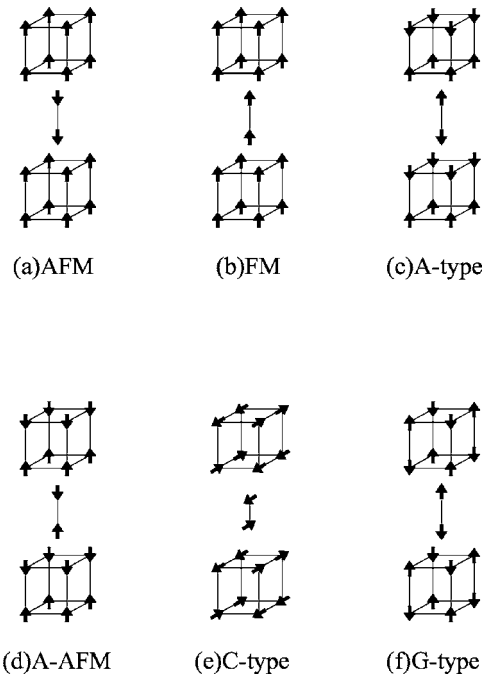

FIG. 1. Schematic diagram for various magnetic states of $La_{2-2x}Sr_{1+2x}Mn_2O_7$ considered in this paper. (a) AFM state, (b) FM state, (c) A-type state, (d) A-AFM state, (e) C-type state, (f) G-type state. Arrows represent the moments of manganese ions.

and the G-type antiferromagnetic state with $d_{3z^2-r^2}$ orbital ordering ($0.92 < x \leqslant 1$). These results are in agreement with the available experimental observations.

To address the various ordering phenomena in the bilayer perovskite, we combine the multiband d-p Hamiltonian $\mathcal{H}_e$ with the generalized Jahn-Teller coupling term $\mathcal{H}_{\mathrm{JT}}$. $\mathcal{H}_e$ has the following form:[17]

$$\begin{aligned}\mathcal{H}_e = & \sum_{im\sigma} \varepsilon^0_{dm} d^\dagger_{im\sigma} d_{im\sigma} + \sum_{jn\sigma} \varepsilon_p p^\dagger_{jn\sigma} p_{jn\sigma} \\ & + \sum_{ijmn\sigma} (t^{mn}_{ij} d^\dagger_{im\sigma} p_{jn\sigma} + \mathrm{H.c.}) \\ & + \sum_{ijnn'\sigma} (t^{nn'}_{ij} p^\dagger_{in\sigma} p_{jn'\sigma} + \mathrm{H.c.}) + \sum_{im} u d^\dagger_{im\uparrow} d_{im\uparrow} d^\dagger_{im\downarrow} d_{im\downarrow} \\ & + \frac{1}{2} \sum_{im\neq m'\sigma\sigma'} \tilde{u} d^\dagger_{im\sigma} d_{im\sigma} d^\dagger_{im'\sigma'} d_{im'\sigma'} \\ & - J_H \sum_{im\sigma\sigma'} d^\dagger_{im\sigma} \boldsymbol{\sigma} d_{im\sigma'} \cdot \mathbf{S}^d_{im} + J_S \sum_{\langle i,j\rangle} \mathbf{S}^t_i \cdot \mathbf{S}^t_j. \end{aligned} \tag{1}$$

$d_{im\sigma}$ and $p_{jn\sigma}$ denote the annihilation operators for an electron of spin σ on Mn-d_m orbital at site i and O-p_n orbital at site j, respectively. ε^0_{dm} and ε_p are their corresponding on-site energies. The splitting of Mn-d orbitals within the octahedra are included in the on-site energy via $\varepsilon^0_d(e_g) = \varepsilon^0_d + 6Dq$, $\varepsilon^0_d(t_{2g}) = \varepsilon^0_d - 4Dq$, ε^0_d is the bare on-site energy of the d orbitals, and $10Dq$ is the crystal-field splitting. t^{mn}_{ij} and $t^{nn'}_{ij}$ are the nearest neighbor hopping integrals for p-d and p-p, which are expressed in terms of Slater-Koster parameters $(pd\sigma)$, $(pd\pi)$, $(pp\sigma)$, and $(pp\pi)$. $\mathbf{S}^d_{im}$ is the total spin operator of the Mn ion extracting the spin operator in orbital m. The parameter J_H is the Hund's coupling constant, $\tilde{u} = u - 5J_H/2$, and u is related to the multiplet averaged d-d Coulomb interaction U via $u = U + (20/9)J_H$. J_S is the superexchange coupling among the neighboring localized t_{2g} moments, which was estimated by Feiner and Oleś for the insulating $LaMnO_3$.[18]

The generalized Jahn-Teller coupling term for the d-orbitals at octahedral sites reads[19]

$$\begin{aligned}\mathcal{H}_{\mathrm{JT}} = \sum_{i\sigma} \Bigg(& -g_1 Q_1(i) \sum_m d^\dagger_{im\sigma} d_{im\sigma} - g_2 \Bigg\{ Q_3(i) d^\dagger_{ixy\sigma} d_{ixy\sigma} \\ & + \left[\frac{\sqrt{3}}{2} Q_2(i) - \frac{1}{2} Q_3(i) \right] d^\dagger_{iyz\sigma} d_{iyz\sigma} + \left[-\frac{\sqrt{3}}{2} Q_2(i) \right. \\ & \left. - \frac{1}{2} Q_3(i) \right] d^\dagger_{izx\sigma} d_{izx\sigma} + (d_{ix^2-y^2\sigma}, d_{i3z^2-r^2\sigma}) \\ & \times \begin{pmatrix} Q_3(i) & Q_2(i) \\ Q_2(i) & -Q_3(i) \end{pmatrix} \begin{pmatrix} d_{ix^2-y^2\sigma} \\ d_{i3z^2-r^2\sigma} \end{pmatrix} \Bigg\} \Bigg). \end{aligned} \tag{2}$$

Here Q_1, Q_2, and Q_3 are the three Jahn-Teller distortion modes. Q_1 is the breathing mode, Q_2 and Q_3 modes are the vibration modes.[20] g_1 and g_2 are the coupling strengths.[19] For the volume conserving modes Q_2 and Q_3, a Jahn-Teller angle can be defined $Q_2 = Q \sin\alpha$ and $Q_3 = Q \cos\alpha$; then $\alpha = 0$, $2\pi/3$, $-2\pi/3$ correspond to the Jahn-Teller distortion axis along the c, a, and b axes.

The above equation set can be solved within the unrestricted Hartree-Fock approximation and real-space recursion method.[19,21,22] In order to investigate all possible magnetic states of $La_{2-2x}Sr_{1+2x}Mn_2O_7$, we have considered various ordered states of an enlarged octuple cell of $La_{2-2x}Sr_{1+2x}Mn_2O_7$ and computed 31 levels for each of the 248 independent orbitals. Our results have been checked for different levels to secure an energy accuracy better than 5 meV.

The parameter set used in our numerical calculations is deduced from the cluster model analysis of the photoemission spectra[17] and from those of the well-studied cubic structured $LaMnO_3$ compound. In this paper, the bare on-site energies of Mn-d and O-p orbitals are taken as $\varepsilon^0_d = -13.0$ eV and $\varepsilon_p = 0$ eV. We choose the crystal-field splitting energy $10Dq = 1$ eV, the on-site Coulomb repulsion and Hund's coupling constant are set at $U = 5.0$ eV and $J_H = 0.8$ eV. The superexchange coupling between the nearest neighbor localized t_{2g} spins is chosen as $J_S = 0.005$ eV.[18] The Slater-Koster parameters are estimated from those of $LaMnO_3$ using the well-known scaling relations,[23] the average bond lengths listed in Ref. 14, and the Slater-Koster parameters of $LaMnO_3$[$(pd\sigma) = -2.0$ eV, $(pd\pi) = 0.922$ eV, $(pp\sigma) = 0.6$ eV and $(pp\pi) = -0.15$ eV]. In order to check the importance of the Jahn-Teller effect, three types of Jahn-Teller distortion modes are considered in our numerical calculation: $[-2\pi/3, 2\pi/3]$, $[0, 0]$, and $[\pi, \pi]$ modes, respectively. The α and β in $[\alpha, \beta]$ mode represent the Jahn-Teller angles for the nearest neighbor octahedral sites. The corresponding orbital orderings are $[d_{3x^2-r^2}, d_{3y^2-r^2}]$, $[d_{3z^2-r^2}, d_{3z^2-r^2}]$, and $[d_{x^2-y^2}, d_{x^2-y^2}]$, respectively. Note that all the Jahn-Teller modes discussed above conserve the cell volume and we use the magnitude of Jahn-Teller distortion $Q = 3.0\%$. The electron-phonon coupling constants are estimated assuming $Z = 1.5$.[19]

With the parameter set given above, we have studied the electronic structures of various spin states with different orbital orderings. Because of the strong coupling within the bilayers and very weak coupling between the bilayers, the AFM state [Fig. 1(a)] and the FM state [Fig. 1(b)] are very close in energy in the whole doping range, as are the A-type state [Fig. 1(c)] and the A-AFM state [Fig. 1(d)]. Below, we concentrate on the states illustrated in Figs. 1(b), 1(c), 1(e), and 1(f) since they are the only states which become the ground state in some of the doping range. For each state, we consider three different types of orbital ordering; there are twelve states in total. The relative energies of these twelve states as a function of doping are plotted in Fig. 2 with respect to that of the FM state with $d_{3z^2-r^2}$ orbital ordering. Our results show that the first magnetic transition takes place between the A-type AFM state and the FM state at doping concentration $x = 0.01$ and the nearest neighbor orbital orderings of both states take the form of $d_{3x^2-r^2}/d_{3y^2-r^2}$ pattern. As doping concentration increases to $x = 0.23$, the magnetic state remains the FM state but the orbital ordering is replaced by $d_{x^2-y^2}$. As the doping concentration increases to $x = 0.34$, the A-type AFM state becomes the ground state again but the orbital ordering remains $d_{x^2-y^2}$. When the doping concentration increases to $x = 0.86$, the C-type AFM state takes place and the orbital ordering keeps the same. The G-type AFM

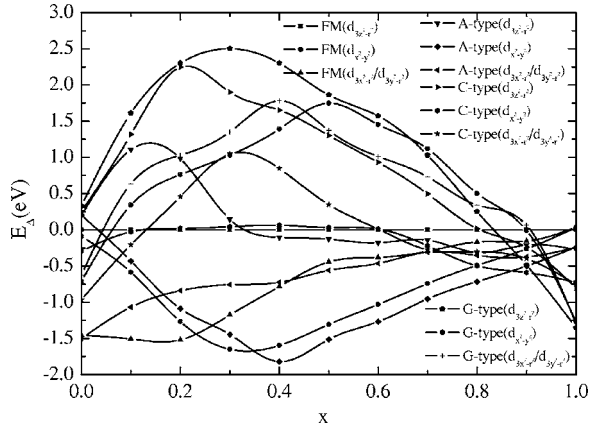

FIG. 2. The doping dependence of relative energies E_Δ per octuple cell. The energy is plotted with respect to that of the FM state with the $d_{3z^2-r^2}$ orbital ordering, twelve spin and orbital ordered states are shown. Other parameters are described in the text.

state becomes the ground state only when doping concentration $x \geqslant 0.92$ and the $d_{3z^2-r^2}$ orbital ordering becomes dominant. In the following, the electronic, magnetic, as well as orbital properties of these possible ground states are discussed briefly.

The first state we are going to present is the A-type AFM state of $La_2SrMn_2O_7$. Similar to the A-type AFM state of $LaMnO_3$, this state is unstable in the absence of Jahn-Teller distortion. However, a sizable Jahn-Teller distortion lifts the degeneracy of two e_g orbitals, the antiferro-orbital ordering $[d_{3x^2-r^2}/d_{3y^2-r^2}]$ favors the in-plane double exchange mechanism and makes this state stable. The total density of states (TDOS) of A-type AFM state is shown in Fig. 3(a). Consistent with the insulator property observed in experiments, Fermi energy ($E_F=0$) is located in the band gap. The analysis of partial densities of states (PDOS) reveals that double peaks around ±4 eV are contributed by the localized t_{2g} orbitals due to exchange field and orbital ordering. The density of states (DOS) immediately above and below the Fermi energy comes from the more itinerant e_g orbitals. Oxygen O-p orbitals are almost full and their DOS lies far below the Fermi energy (−12 eV, 6 eV). The occupancy of the d bands is $n_d=4.503$, which is larger than 4 due to the charge transfer from O-p to Mn-d orbitals. The corresponding magnetic moment is $\mu_d=3.95\mu_B$.

For a small to moderate doping concentration $0.01 < x \leqslant 0.23$, the A-type AFM ground state is replaced by the FM ground state. The ferromagnetic state has the $d_{3x^2-r^2}/d_{3y^2-r^2}$ orbital so that the double exchange mechanism is effective for the extra electrons in e_g orbitals and the system's kinetic energy is minimized. The total densities of states for doping concentration $x=0.1$ are plotted in Fig. 3(b). It is found that there is a small but finite density of states at Fermi energy ($E_F=0$) and the system becomes metallic. The spectral positions of Mn-d-t_{2g} orbitals remains the same since the exchange field is not much affected, as well as the O-p orbitals, though they are slightly polarized due to the small induced moment. The dramatic change takes place for the e_g-orbital related bands; they are significantly broadened due to increased itineracy after doping. In agreement with experiment, compounds in a ferromagnetic state show a half-metal feature and only one of the polarized bands crosses the Fermi energy. The electron occupancy is $n_d=4.45$, the corresponding magnetic moment is $\mu_d=3.89\mu_B$.

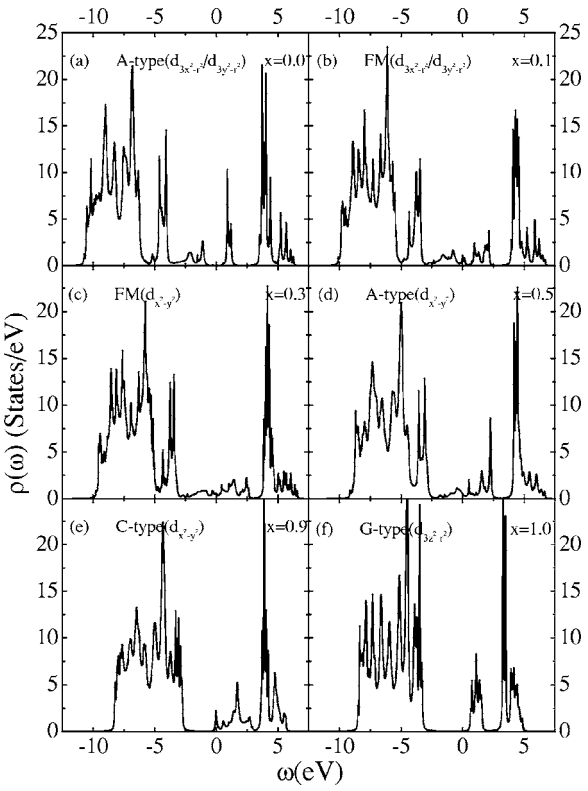

FIG. 3. The total densities of states of six ground states. (a) A-type AFM $[d_{3x^2-r^2}/d_{3y^2-r^2}]$ at $x=0$; (b) FM $[d_{3x^2-r^2}/d_{3y^2-r^2}]$ at $x=0.1$; (c) FM $[d_{x^2-y^2}]$ at $x=0.3$; (d) A-type AFM $[d_{x^2-y^2}]$ at $x=0.5$; (e) C-type AFM $[d_{x^2-y^2}]$ at $x=0.9$; (f) G-type AFM $[d_{3z^2-r^2}]$ at $x=1$. Other parameters are described in the text.

As doping increases further to the range $0.23 < x \leqslant 0.34$, the ground state of the system remains a FM state but the orbital ordering changes to a $d_{x^2-y^2}$ pattern. As indicated in Fig. 3(c), e_g-orbital electrons become more itinerant and form broader bands in the range near Fermi energy. The TDOS resemble that of Fig. 3(b) and Fermi energy moves further down into the valence band. This state also possesses the half-metal feature with fully polarized DOS at the Fermi energy. The electron occupancy and magnetic moment are $n_d=4.35$ and $\mu_d=3.73\mu_B$, respectively. When $0.34 < x \leqslant 0.86$, the A-type antiferromagnetic state replaces the FM state as the ground state of the system. However, the orbital ordering still keeps the $d_{x^2-y^2}$ pattern as was observed in the magnetic Compton profile.[11,15] Its TDOS [Fig. 3(d)] is quite similar to that shown in Fig. 3(a) except that the band gap is very much reduced and this state is a metallic antiferromagnet. Due to the antiferromagnetic ordering, the t_{2g} related bands are more localized than ferromagnetic state, but the e_g related bands are even more extended across the whole region of Fermi energy. The electron occupancy is $n_d=4.26$ and magnetic moment is $\mu_d=3.58\mu_B$.

When more and more La are substituted by Sr, more electrons in the e_g orbitals are removed from system. This sub-

stitution dramatically prohibits the ferromagnetic coupling between Mn ions coming from the double exchange, and a superexchange interaction between the localized t_{2g} orbitals becomes dominant. Following this trend, at the very large doping range $0.86 < x \leqslant 0.92$, the doped bilayer perovskite takes the C-type antiferromagnetic state with $d_{x^2-y^2}$ orbital ordering. The TDOS shown in Fig. 3(e) suggests that the compound is still a metal from the band picture, the electron occupancy is $n_d=4.04$, and magnetic moment is $\mu_d = 3.20\mu_B$. As the doping concentration approaches 1, the ground state of $La_{2-2x}Sr_{1+2x}Mn_2O_7$ is replaced by the G-type AFM, which was originally proposed by Mitchell *et al.*.[16] The orbital ordering is dominated by the $d_{3z^2-r^2}$ pattern, TDOS at $x=1$ is shown in Fig. 3(f). Unlike all other states presented previously, the nearest neighbor antiferromagnetic state is magnetically modulated along all crystal axes, and such modulation causes band folding and reduced band widths. As is evident from Fig. 3(f), this state is an insulator with a large band gap. The electron occupancy is $n_d=3.98$ and the corresponding magnetic moment is $\mu_d=3.09\mu_B$.

In summary, we have studied in this paper the spin and orbital orderings of various magnetic ground states of $La_{2-2x}Sr_{1+2x}Mn_2O_7$ as a function of doping. Our results show that the A-type AFM insulator of the undoped parent $La_2Sr_1Mn_2O_7$ compound is stabilized by the Jahn-Teller distortion. As doping increases, the ground state of $La_{2-2x}Sr_{1+2x}Mn_2O_7$ takes consecutively the FM state with $d_{3x^2-r^2}/d_{3y^2-r^2}$ orbital ordering, the FM state with $d_{x^2-y^2}$ orbital ordering, the A-type AFM state with $d_{x^2-y^2}$ orbital ordering, the C-type AFM state with $d_{x^2-y^2}$ orbital ordering, and finally the G-type AFM state with $d_{3z^2-r^2}$ orbital ordering.

This work was supported in part by the State Key Program for Basic Research of China (Grant No. 2004CB619003). We wish to acknowledge the partial financial support from the NNSFC under Grant No. 10474040, 10334090, and "Excellent Youth Foundation" (Grant No. 10025419).

[1] R. von Helmolt, J. Wecker, B. Holzapfel, L. Schultz, and K. Samwer, Phys. Rev. Lett. **71**, 2331 (1993).
[2] S. Jin, T. H. Tiefel, M. McCormack, R. A. Fastnacht, R. Ramesh, and L. Chen, Science **264**, 413 (1994).
[3] A. Asamitsu, Y. Moritomo, Y. Tomioka, T. Arima, and Y. Tokura, Nature **373**, 407 (1995).
[4] *Colossal Magnetoresistance, Charge Ordering and Related Properties of Manganese Oxides*, edited by C. N. R. Rao and B. Raveau (World Scientific, Singapore, 1998).
[5] *Colossal Magnetoresistive Oxides*, edited by Y. Tokura (Gordon and Breach, New York, 2000).
[6] See, e. g., Y. Tokura and N. Nagaosa, Science **288**, 462 (2000).
[7] Y. Moritomo, A. Asamitsu, H. Kuwahara, and Y. Tokura, Nature **380**, 141 (1996).
[8] D. N. Argyriou, J. F. Mitchell, P. G. Radaelli, H. N. Bordallo, D. E. Cox, M. Medarde, and J. D. Jorgensen, Phys. Rev. B **59**, 8695 (1999)
[9] T. G. Perring, G. Aeppli, T. Kimura, Y. Tokura, and M. A. Adams, Phys. Rev. B **58**, R14693 (1998).
[10] T. Kimura, Y. Tomioka, H. Kuwahara, A. Asamitsu, M. Tamura, and Y. Tokura, Science **274**, 1698 (1996).
[11] C. D. Ling, J. E. Millburn, J. F. Mitchell, D. N. Argyriou, J. Linton, and H. N. Bordallo, Phys. Rev. B **62**, 15096 (2000).
[12] X. Y. Huang, O. N. Mryasov, D. L. Novikov, and A. J. Freeman, Phys. Rev. B **62**, 13318 (2000).
[13] P. K. de Boer and R. A. de Groot, Phys. Rev. B **60**, 10758 (1999).
[14] J. F. Mitchell, D. N. Argyriou, J. D. Jorgensen, D. G. Hinks, C. D. Potter, and S. D. Bader, Phys. Rev. B **55**, 63 (1997).
[15] A. Koizumi, S. Miyaki, Y. Kakutani, H. Koizumi, N. Hiraoka, K. Makoshi, N. Sakai, K. Hirota, and Y. Murakami, Phys. Rev. Lett. **86**, 5589 (2001).
[16] J. F. Mitchell, J. E. Millburn, M. Medarde, S. Short, J. D. Jorgensen, and M. T. Fernández-Díaz, J. Solid State Chem. **141**, 599 (1998).
[17] T. Mizokawa and A. Fujimori, Phys. Rev. B **53**, R4201 (1996); **54**, 5368 (1996); Phys. Rev. B **51**, 12880 (1995).
[18] Louis Felix Feiner and Andrzej M. Oleś, Phys. Rev. B **59**, 3295 (1999).
[19] Qinfang Zhang, Weiyi Zhang, and Zhengsheng Jiang, Phys. Rev. B **72**, 144415 (2005).
[20] I. O. Troyanchuk, S. V. Trukhanov, H. Szymczak, and K. Bärner, J. Phys.: Condens. Matter **12**, L155 (2000).
[21] V. Heine, R. Haydock, and M. J. Kelly, in *Solid State Physics: Advances in Research and Applications*, edited by H. Ehrenreich, F. Seitz, and D. Turnbull (Academic, New York, 1980), Vol. 35, p. 215.
[22] R. Haydock and C. M. M. Nex, J. Phys. C **17**, 4783 (1984).
[23] Walter A. Harrison, *Electronic Structure and the Properties of Solids* (W. H. Freeman and Company, San Francisco, 1980).